Green water-induced spinel heterostructure interface enabling high performance lithium and manganese rich oxides

Wenqiang Tu,[1] Xianshu Wang,[1] Wenying Tian,[1] Yunan Zhou,[1] Cuiping Han,[2,*] Chuan Li,[3] Feiyu Kang,[1] Baohua Li[1,*]

1 Shenzhen Key Laboratory of Power Battery Safety Research and Shenzhen Geim Graphene Center, Tsinghua Shenzhen international Graduate School (SIGS), Tsinghua University, Shenzhen 518055, China.

Email: libh@mail.sz.tsinghua.edu.cn *(B. Li)*

2. Faculty of Materials Science and Engineering, Shenzhen Institute of Advanced Technology, Chinese Academy of Sciences, Shenzhen, 518055, China.

E-mail: cp.han@siat.ac.cn *(C. Han)*

3. Department of Materials Science and Engineering, City University of Hong Kong, 83 Tat Chee Avenue, Kowloon, Hong Kong 999077, China.

Experimental section

Preparation of cathodes

The $Li_{1.2}Mn_{0.55}Ni_{0.15}Co_{0.1}O_2$ (OLLO) was prepared through cooperated-precipitate (CP) method, as our previous works.[1, 2] Typically, the $MnSO_4•H_2O$ (Aladdin, AR), $NiSO_4•6H_2O$ (Aladdin, AR), $CoSO_4•6H_2O$ (Aladdin, AR) with stoichiometry mol ratio were dissolved into water to prepare solution A. $LiOH·H_2O$ (Aladdin, AR) and $NH_3·H_2O$ (Aladdin, AR) ($LiOH·H_2O$ is stoichiometry for precipitate, NH_3 is 10% mol of LiOH) were mixed to prepare solution B. Then both solution A and solution B were pumped into a flask under consistent stirring in N_2 gas atmosphere. After completed precipitate, the mix solutions were filtered to get the hydroxide precursors and then dried at 80 ℃ in vacuum drying oven. The hydroxide precursors were mixed with $LiOH·H_2O$ (5% excess by the stoichiometry mol ratio) by grinding and then annealed at 500 ℃ for 5h and reannealed at 900 ℃ for 10h in air atmosphere. After cooling down, the pristine $Li_{1.2}Mn_{0.55}Ni_{0.15}Co_{0.1}O_2$ (OLLO) powders were obtained.

0.2g OLLO powders were put into a 50 mL Teflon bottle with 35 mL of deionized water. Then

the Teflon bottle filled with OLLO and water were sealed and then heated at 150 ℃ for 10h or 200 ℃ for 10h. Afterward, the treated particles were washed and dried in 80 ℃ oven. Then the treated powders were heated at 500 ℃ for 3h to obtain the SLLO with spinel heterostructure layer. The SLLO powders hydrothermally treated at 150 and 200°C with 10h were marked as SLLO-150 and SLLO-200, respectively. And the SLLO-150 will mainly discussed in the text.

The cathode electrodes were prepared by coating the slurries of active materials, Super P carbon, polyvinylidene fluoride (PVDF) (by weight ratio of 8:1:1) on Al foil. The slurries were dried at 80 ℃ oven for 6h and 120 ℃ vacuum drying oven for 12h. At last, the mass loading of active materials is ~2 mg cm^{-2}. The electrolyte is the 1.2 M LiPF$_6$ dissolved in the mixed solvents of ethylene carbonate (EC), dimethyl carbonate (DMC) and diethyl carbonate (DEC) (on volume ratio=1:1:1, purchased from the Sigma-Aldrich). The half cells were assembled with 2025-coin cell with OLLO/SLLO cathode, Celgard 2400 separator and Li metal anode in glove box with Ar gas in which the concentrations of water and oxygen were less than 10 ppm.

Electrochemical and physical treatments

The cyclic performances were conducted on a Land cell test system (Land CT2001, China). All the cells were performed at the following procedure: the cells were charged/discharged at 0.1 C current rate (1C= 200 mA g^{-1}) between 2-4.8V (vs. Li$^+$/Li) for the initial three cycles and then at other current rates for the subsequent cycles. The electrochemical impedance spectroscopy (EIS) was measured on Solartro 1470E instrument (England) at the 5 mV amplitude from 10^5 Hz to 0.1 Hz, and measurements were carried out in the full discharged condition (~2 V). Cyclic voltammetry (CV) was measured on Solartro 1480 between 2-4.8V with various scan rates.

The morphology and microcrystal structure of OLLO and SLLO were measured by a field emission scanning electron microscope (HITAXHI SU8010) and a high -resolution transmission electron microscope (FEI Tecnai G2 F30), respectively. X-ray diffraction (XRD, Bruker D8 Advance, Germany) evaluated the crystal structure lattice and performed at 40 KV and 40 mA using Cu Ka radiation (λ=1.5405 nm) between the 2θ range from 10 to 90º. Raman spectroscopy was performed to analyze the crystal structure evolution with a LabRAM HR800 (Horiba) using green laser (532nm) with the 500 nm diameter and 1 um depth length diffraction spot. To ensure reproducibility, 5 spots were measured on each sample. X-ray photoelectron spectroscopy (XPS)

was performed to analyze the evolution of valence states of elements. XPS were tested on PHI 5000 Versa Probe II with a monochromatic Al Kα X-ray source (excitation energy=1468.6 eV). The data was collected from an X-Ray spot size of 400 um and the binding energy was corrected based on the C1s signal at 284.8 eV. Chemical composition of active material powders and the concentration of ions in H_2O solution after hydrothermal reaction were carried out by using an inductively coupled plasma-atomic emission spectrometer (ICP-AES, Arcos II MV).
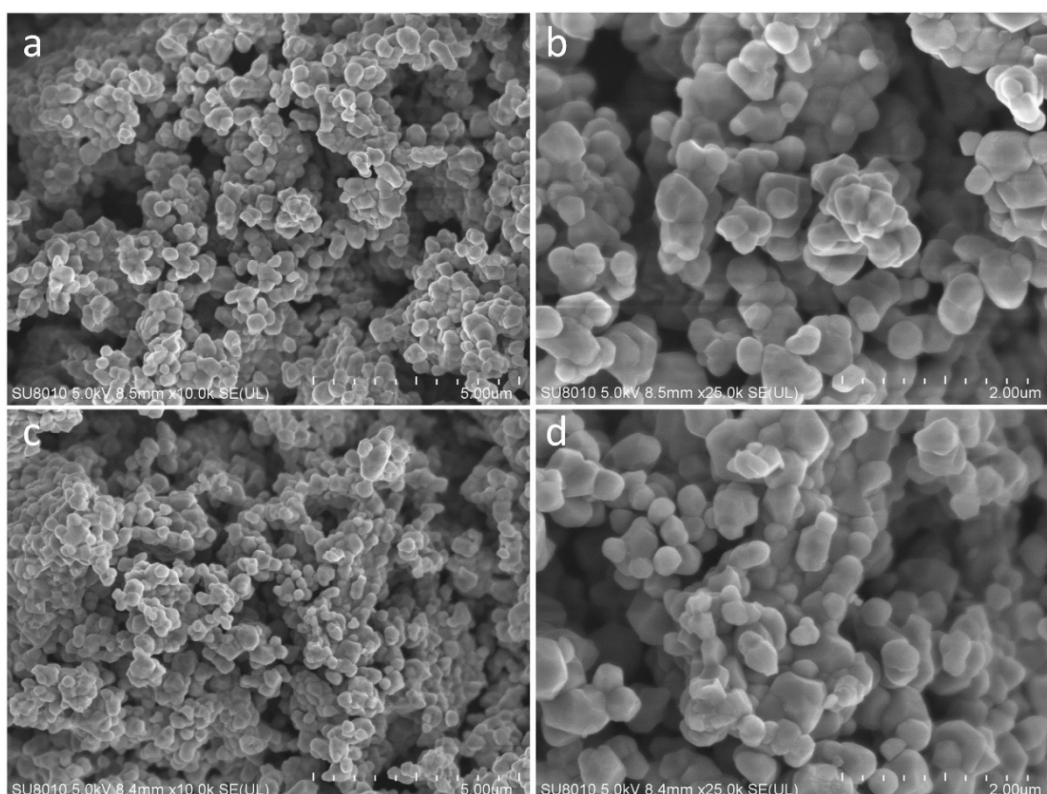

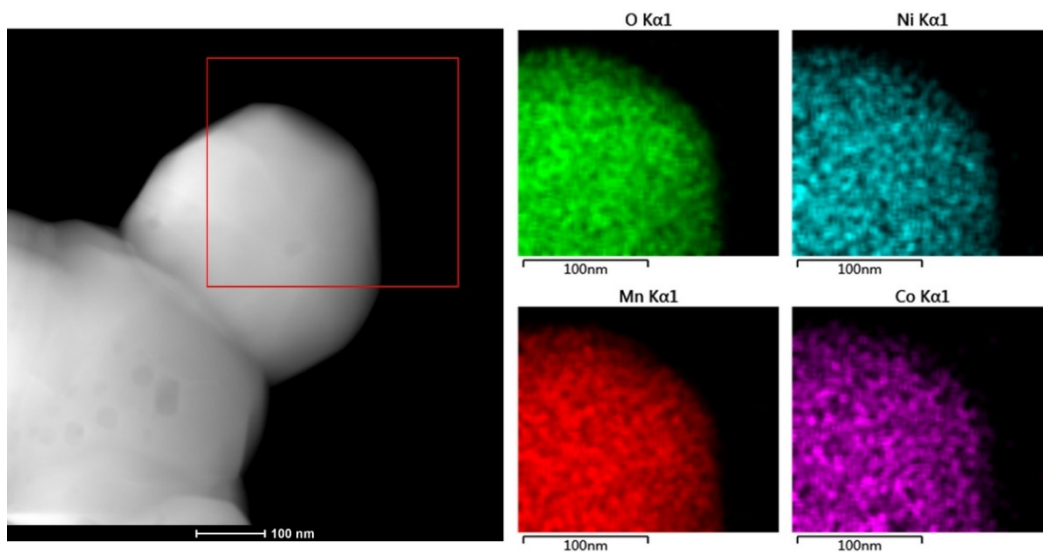Fig. S1 The SEM images of OLLO (a, b) and SLLO (c, d).

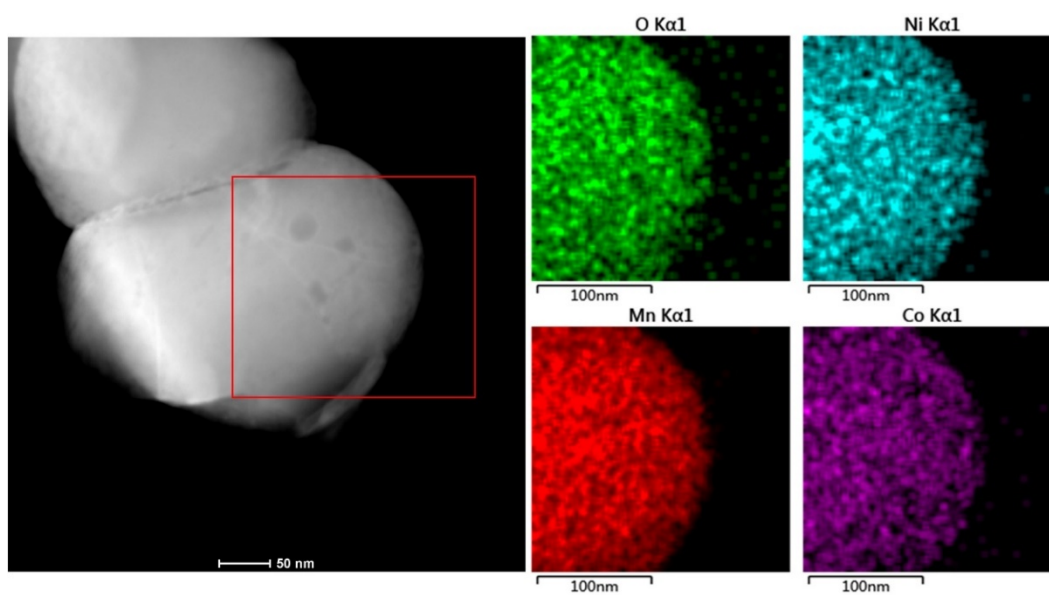Fig. S2 The element mapping images of OLLO.

Fig. S3 The element mapping images of SLLO.

As shown in Fig. S2 and S3, the transition metal elements are homogeneously distributed in OLLO and SLLO particles, which suggests that the spinel modification doesn't obviously change the distribution of transition metals. The results are consistent with the results in XRD patterns and SEM images of OLLO and SLLO.
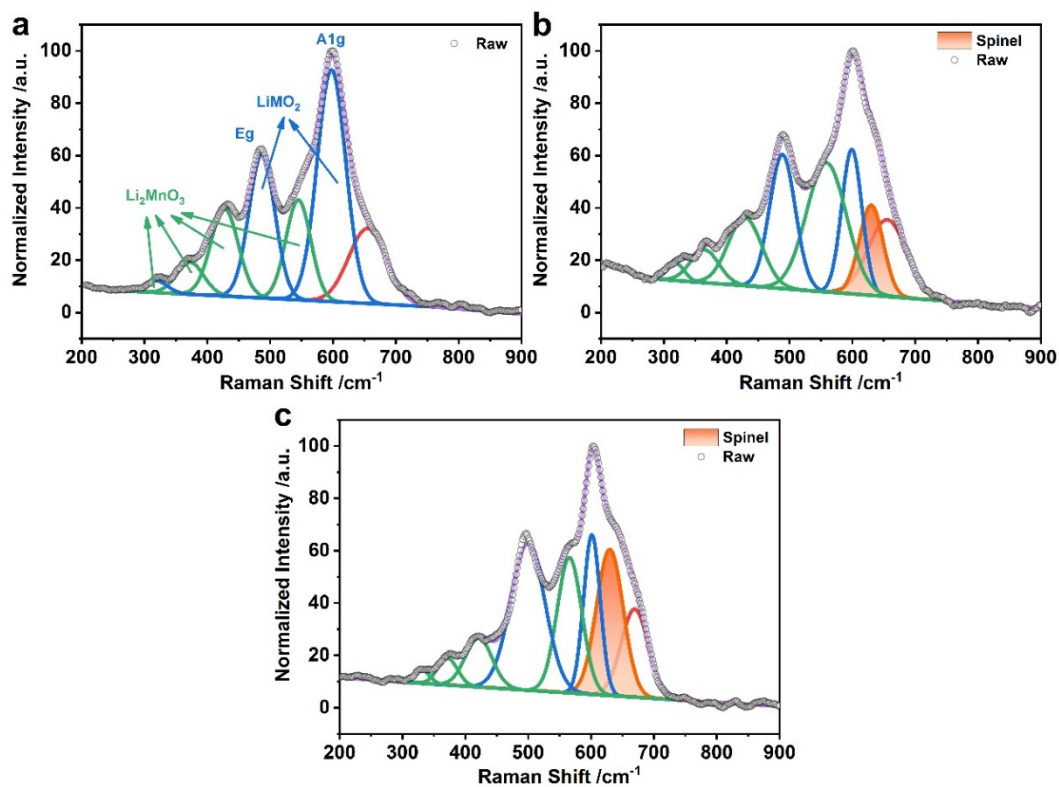
Fig. S4 The Raman spectra of OLLO (a), SLLO-150 (b) and SLLO-200 (c).

As shown in Fig. S4, obvious shoulder peaks at about 630 cm^{-1} can be observed in SLLO-150 and SLLO-200 samples. The additional shoulder peak is related to spinel structure, which suggests that spinel heterostructure layer was successfully introduced on SLLO surface. Compared with SLLO-150, the intensities of spinel phase at 630 cm^{-1} in SLLO-200 increased, which suggests that the contents of introducing spinel phase are easily controllable by reaction temperature.
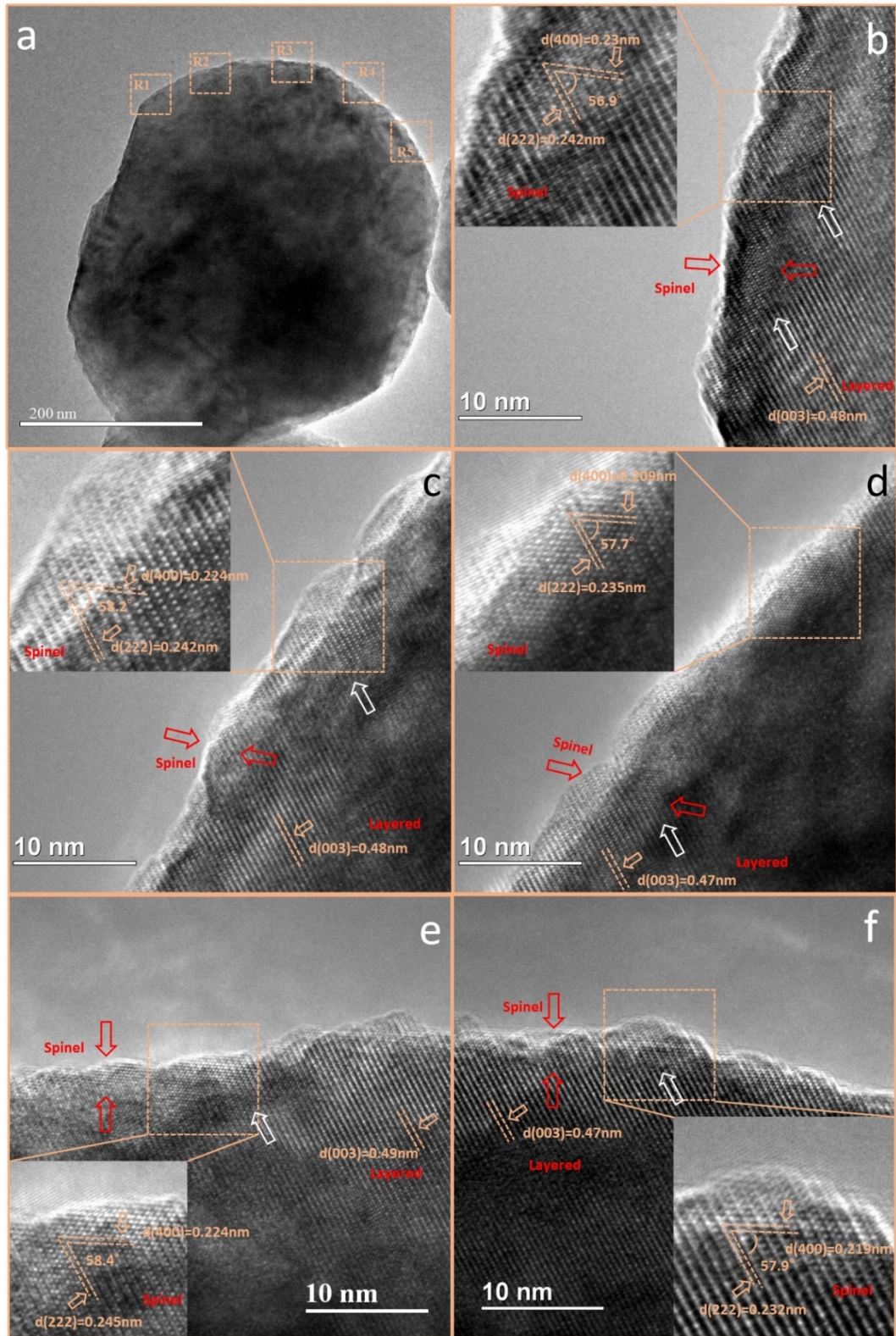
Fig. S5 The HRTEM images of SLLO. HRTEM images (b, c, d, e, and f) are the corresponding magnified images from the orange box (R1, R2, R3, R4 and R5, respectively) in image (a).

As shown in Fig. S5, the HRTEM images (b-f) display obvious spinel interface with about 5-7nm thickness (marked by the red arrows) on the margin areas of SLLO. As marked by the white arrows, the TM atoms (bright dots) occupy the Li layers, which demonstrates the phase transformation from layered to spinel phase and is consistent with that in Fig. 4. Moreover, the spinel heterostructure layer covers almost the entire margin areas of SLLO (shown by the orange boxes (R1-R5)), which suggests that the spinel interfacial layer is uniform on the SLLO surface.
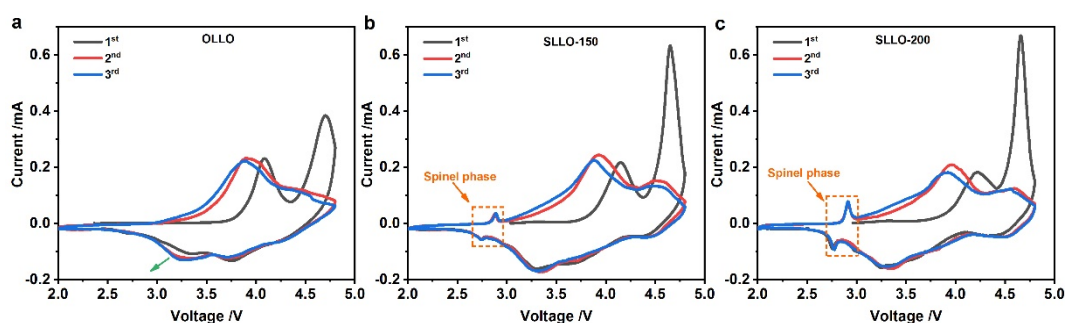

Fig. S6 The CV curves of OLLO (a), SLLO-150 (b) and SLLO-200 (c) at 0.1 mV s^{-1} rate.

As shown in Fig. S6, there are two main peaks in the first charge profile, which are related to the oxidation of $Ni^{2+/4+}/Co^{3+/4+}$ (~4.25 V) and Li_2MnO_3 activation (~4.65 V), respectively. And in the subsequently discharge profiles, there are three main peaks, which are corresponded to the lithiation of tetrahedral side (~4.5 V) and the lithiation of octahedral side accompanying with the reduction of $Ni^{4+/2+}/Co^{4+/3+}$ (~3.75V) and $Mn^{4+/3+}$ (~3.25 V, aroused by the Li_2MnO_3 activation). In the 2nd and 3rd charge process, the peaks at about 4.0 V are related to the oxidation of $Ni^{2+/4+}$, $Co^{3+/4+}$ and $Mn^{3+/4+}$ (aroused by the Li_2MnO_3 activation). However, in the CV profiles of SLLO-150 and SLLO-200, an additional pair of redox peaks at ~2.75 V (Fig. S6b and d) is observed, corresponding to the spinel heterostructure layer on SLLO surface. Compared with SLLO-150, the intensities of peaks in ~2.75 V in SLLO-200 are larger, which suggests that the contents of introduced spinel phase can be easily controlled by reaction temperature. As displayed in Fig. S6, the intensities of redox peaks of SLLO are larger than that of OLLO, which demonstrates that the SLLO samples have higher reactivity, resulting into larger capacity. As marked by the green arrow in Fig. S6a, the intensities of peaks at ~3.25 V are dramatically increased, which can be related to the phase transformation from layered

to spinel after Li_2MnO_3 activation. However, the slight changes of peaks (~3.25 V) in SLLO demonstrate more stable crystal structure after introducing spinel heterostructure layer on SLLO.
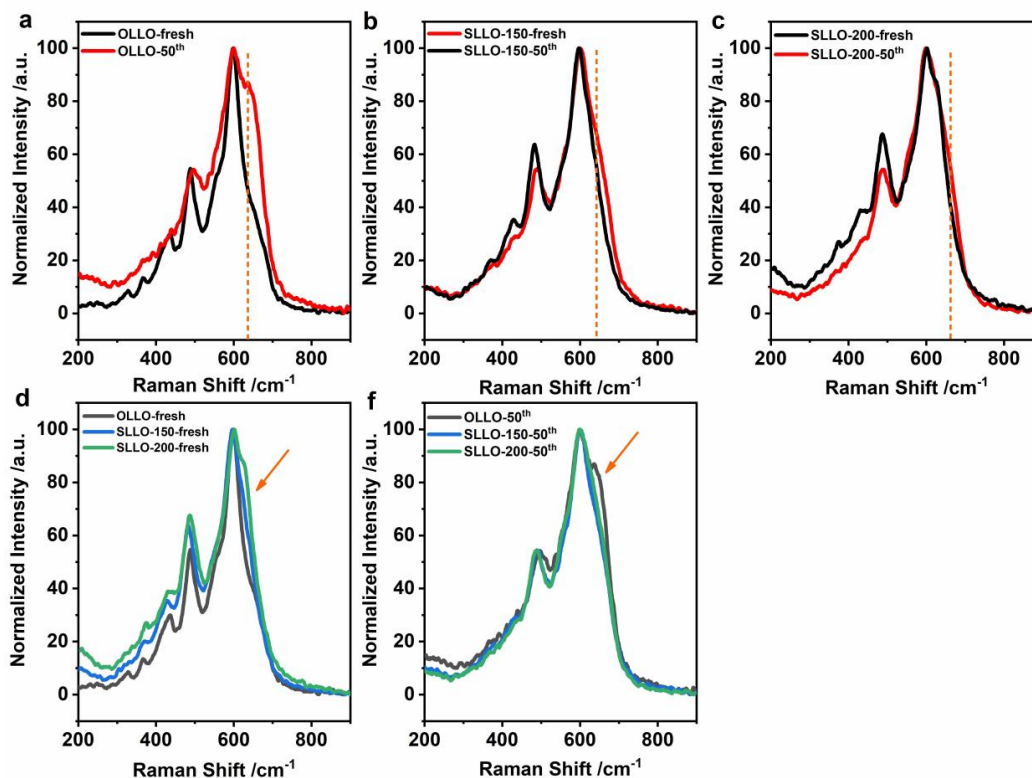

Fig. S7 The Raman spectra of fresh and cycled cathode electrodes of OLLO, SLLO-150 and SLLO-200.

As shown in Fig. S7a, the intensities of shoulder peak at ~630 cm^{-1} (related to the spinel phase) were obviously increased in OLLO after 50 cycles, which demonstrates that serious phase transformation from layered to spinel phase proceed during long-time cycling. Differently, the changes of shoulder peak (~630 cm^{-1}) in SLLO-150 and SLLO-200 are much slightly (Fig. S7b and c). Despite the intensities of shoulder peak (related to spinel phase) in fresh OLLO were less than that in fresh SLLO (marked by the orange arrow in Fig. S7d), the intensities of shoulder peak in cycled OLLO was still higher than that in cycled SLLO (marked by the orange arrow in Fig. S7f), which means that more transformed spinel like phases existed in cycled OLLO. These results suggest that phase transformation were suppressed after introducing spinel heterostructure layer on SLLO surface, which is favorable to sustaining better cycling performance.
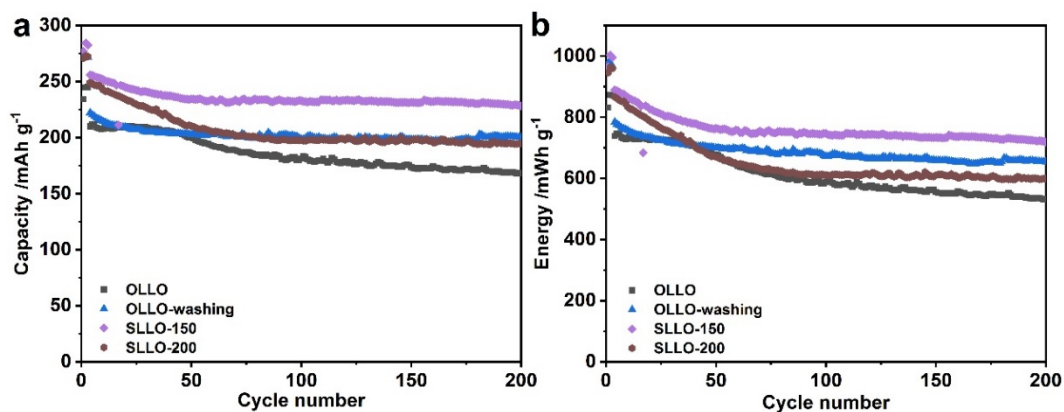
Fig. S8 The cyclic stability performances of original and spinel modified cathodes.

As displayed in Fig. S8, the SLLO-150 delivered the best electrochemical performances and therefore be act as the main discussing object in the texts. Compared with SLLO-150, the cyclic stability of SLLO-200 decreased, which suggests that the content of introducing spinel phase is critical to the performances of SLLO, and introducing too much spinel phase can dramatically decrease the energy density of SLLO.
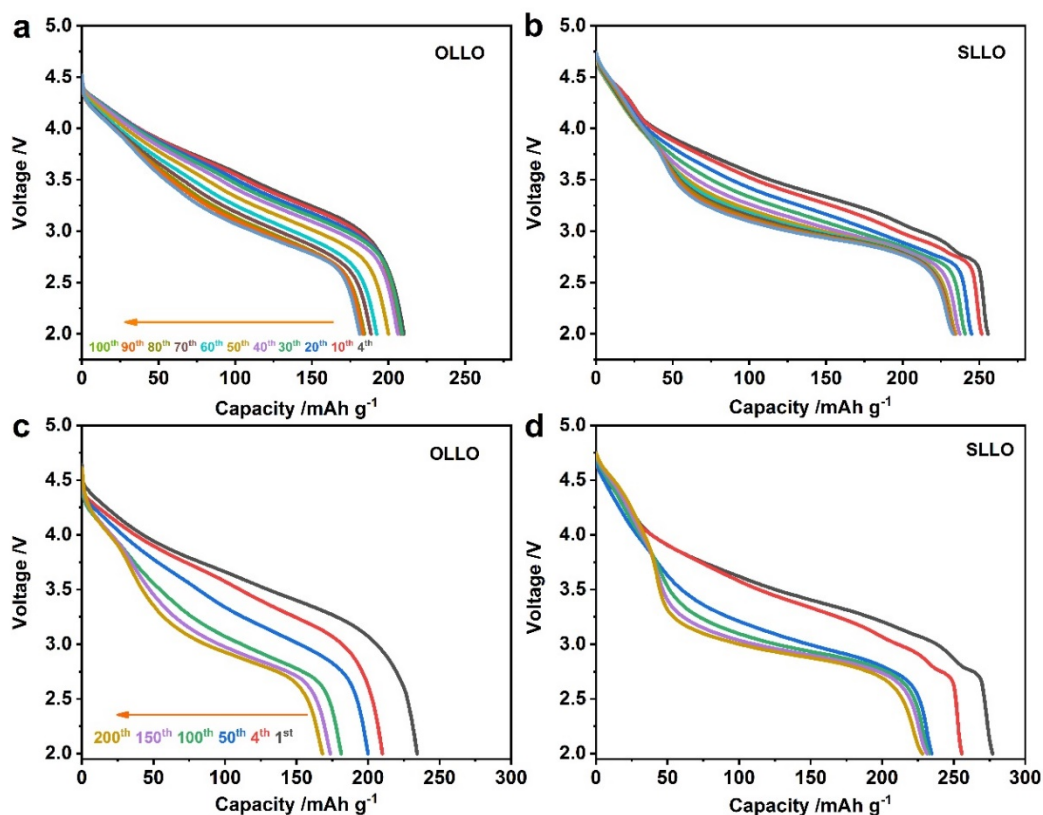

Fig. S9 The selected discharge profiles of OLLO and SLLO.
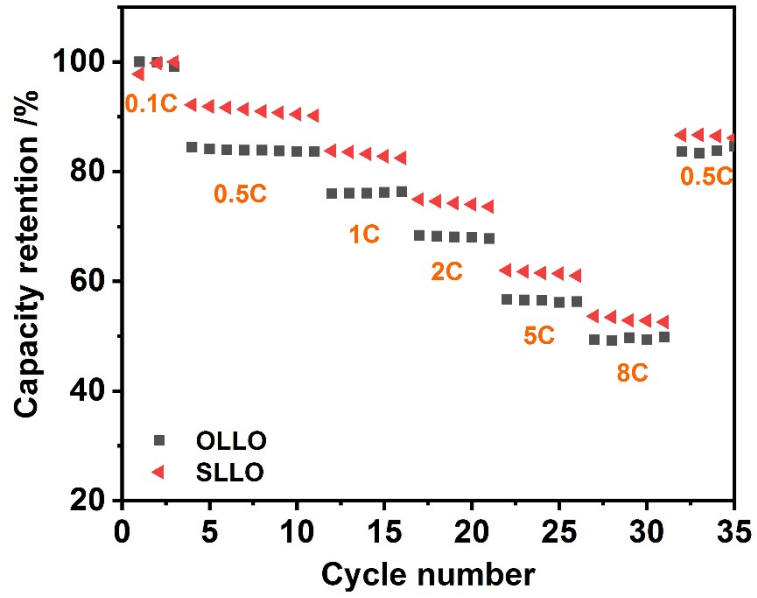
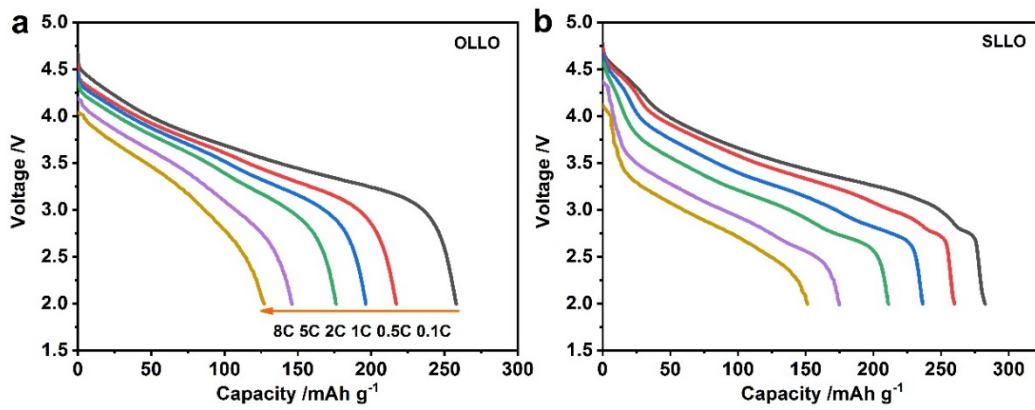Fig. S10 The capacity retention of OLLO and SLLO at various current rate.

Fig. S11 The discharge profiles of OLLO (a) and SLLO (b) at various current rate.
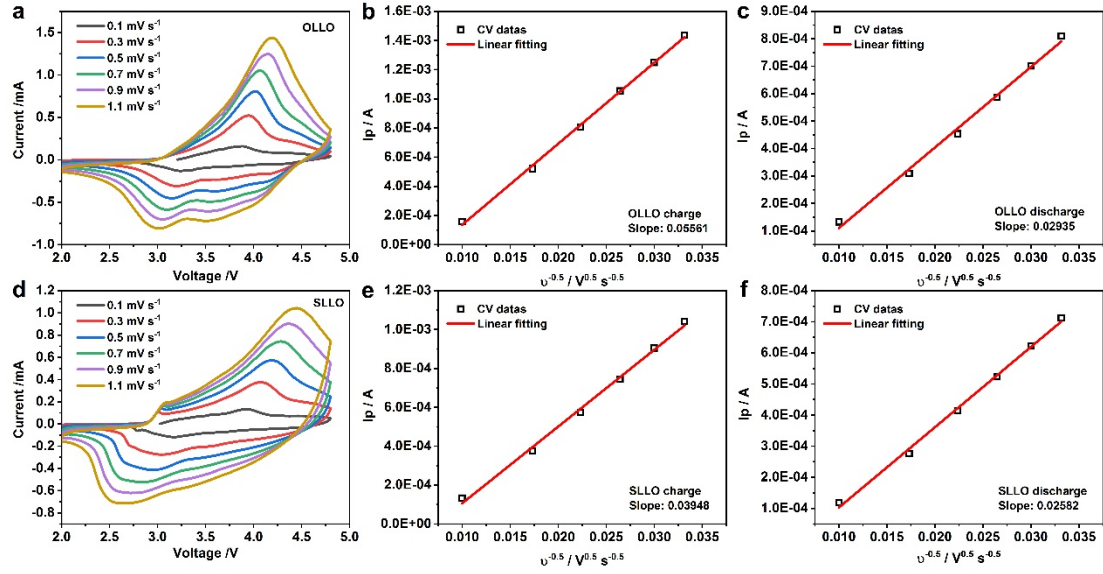
Fig. S12 The CV curves of OLLO (a) and SLLO (b) at various scan rate. The oxidic and reductive peak current densities (Ip) as a function of the square root of the scan rate υ for OLLO (b, c) and SLLO (e, f), respectively.

The D_{Li}^+ can be analyzed by CV profiles at different scan rate. In a diffusion-controlled process, the peak currents (I_p) of certain potential are proportional relationship with the square root of the scan rate ($υ^{0.5}$).[3, 4] Therefore, the diffusion coefficient can be calculated by the Randles-Sevick equation (E1):

$$I_p = 0.4463nFSC(nFυD/RT)^{0.5} \qquad (E1)$$

Where, n is the number of transferred electrons, S is the electrode area, C is the concentration of lithium ions, F is the Faraday constant, D is the diffusion coefficient of Li^+.

Because the value of S and C in Randles-Sevick equation are difficult to determine, therefore it is more valuable to analyze D_{Li}^+ through the relative values of deintercalation and intercalation diffusion coefficient in the same electrode including the same S and C value. Here, we calculated the D for the oxidation peak at ~4.0 V and reduction peak at ~2.75 V. According to the Randles-Sevick equation, the D_{Li}^+ relative values of de-lithiation and lithiation are equal to the squared ratio of slope in charge and discharge process. Therefore, the Li^+ diffusion coefficient decreased by 72.14% for OLLO in the lithiation process compared to de-lithiation process, while is only 57.23% for SLLO, which suggesting the higher lithium-ion diffusion dynamic for SLLO compared with OLLO.

Table S1 Results of ICP-AES tests for OLLO and SLLO.

Sample	Li	Mn	Ni	Co	Ratio of Li:TM
Stoichiometric ratio	1.2	0.55	0.15	0.1	1.5
OLLO	1.1997	0.5403	0.1496	0.1	1.5188
SLLO-150	1.1296	0.5393	0.1499	0.1	1.4313
SLLO-200	1.0926	0.5528	0.1502	0.1	1.3606

Form the results of ICP-AES tests, we can confirm that the chemical formulas of OLLO, SLLO-150 and SLLO-200 are $Li_{1.2}Mn_{0.54}Ni_{0.15}Co_{0.1}O_2$, $Li_{1.13}Mn_{0.54}Ni_{0.15}Co_{0.1}O_2$ and $Li_{1.09}Mn_{0.55}Ni_{0.15}Co_{0.1}O_2$, respectively. It is demonstrates that the contents of Li^+ in SLLO dramatically decreased after Li^+/H^+ ions exchange reaction.

Table S2 The concentrations of Li^+ and TM ions in H_2O solutions after hydrothermal reaction.

Sample	Li ppm	Mn ppm	Ni ppm	Co ppm
SLLO-150	40.725	0	0	0
SLLO-200	52.79	0	0	0

The components of ions in H_2O solutions demonstrate that Li^+/H^+ ions exchange reactions occurred in the hydrothermal process. In addition, the concentration ratio of Li^+ in H_2O solutions is 0.771 that was close to the Li^+ loss ratio (0.636) in chemical formulas of SLLO-150 and SLLO-200. These results suggest that only Li^+/H^+ ions exchange reaction proceeded during hydrothermal reaction, afterwards, layered Li-defected interface formed on the SLLO surfaces.

Table S3 The lattice parameters from the Rietved Refinements through XRD patterns of OLLO and SLLO.

Sample	R-3m		C2/m			Difference	
	a	c	a	b	c	Rwp	Rp
OLLO	2.856362	14.248458	4.954577	8.526291	5.039709	4.46%	3.3%
SLLO	2.857970	14.306418	4.954576	8.578734	5.036594	5.08%	3.66%

Reference

1. W. Tu, Y. Wen, C. Ye, L. Xing, K. Xu and W. Li, *Energy Environ. Mater.*, 2020, **3**, 19-28.
2. C. C. Ye, W. Q. Tu, L. M. Yin, Q. F. Zheng, C. Wang, Y. T. Zhong, Y. G. Zhang, Q. M. Huang, K. Xu and W. S. Li, *J. Mater. Chem. A*, 2018, **6**, 17642-17652.
3. X. D. Zhang, J. L. Shi, J. Y. Liang, Y. X. Yin, J. N. Zhang, X. Q. Yu and Y. G. Guo, *Adv. Mater.*, 2018, **30**, 1801751.
4. Y. Zheng, L. Chen, Y. F. Su, J. Tan, L. Y. Bao, Y. Lu, J. Wang, R. J. Chen, S. Chen and F. Wu, *J. Mater. Chem. A*, 2017, **5**, 24292-24298.